Electrochemical Reactions of Lithium with Transition Metal Nitride Electrodes

Zheng-Wen Fu,* Ying Wang, Xiao-Li Yue, Shang-Li Zhao, and Qi-Zong Qin

Laser Chemistry Institute, Department of Chemistry, Fudan University, Shanghai 200433, P.R. China

Received: April 28, 2003; In Final Form: November 10, 2003

Novel transition metal nitrides of Co_3N and Fe_3N thin films have been successfully fabricated by combining reactive pulsed laser deposition and DC discharge in a nitrogen ambient. The electrochemical reactions of lithium with Co_3N and Fe_3N thin film electrodes were first investigated by the galvanostatic discharge and charge, cyclic voltammetry, and the in-situ spectroelectrochemical measurements. These thin film electrodes exhibited reversible discharge capacities ranging from 324 mAh/g to 420mAh/g. The structure, morphology, and composition of the as-deposited, lithiated, and delithiated Co_3N and Fe_3N thin films have been characterized by X-ray diffraction (XRD), X-ray photoelectron spectroscopy (XPS), and scanning electron microscopy (SEM). The observed diffraction peaks from metal Co(111) and Fe(110) in the lithiated thin films showed well crystallinity of transition metallic Co and Fe formed by Li reacted with Co_3N and Fe_3N, respectively, which could further be confirmed by their XPS spectra. We proposed a new reaction mechanism, in which part of the transition metallic Co and Fe formed during the first discharging is nitrided and another part as an active spectator may play a major role in driving the decomposition and formation of Li_3N during the subsequent electrochemical reaction.

Introduction

Since the transition metal oxides were reported as anode materials of Li ion batteries,[1−3] the electrochemical properties of transition metal compounds have been widely investigated. Besides metal oxides, Pralong et al. studied the lithium uptake and extraction in the metal phosphide of CoP_3,[4] and their data exhibited a reversible capacity of 400 mAh/g at an average potential of 0.9 V vs Li/Li^+. Ternary lithium transition metal nitrides such as $LiMnN_2$, $Li_{3-x}M_xN$(M = Co, Ni), $Li_{2.7}Fe_{0.3}N$, and $Li_{2.6}Co_{0.4}N$[5−7] have been found to be a series of the most promising negative electrodes, and provided reversible capacity between 400 and 760 mAh/g. The excellent electrochemical performances of $Li_{2.7}Fe_{0.3}N$ and $Li_{2.6}Co_{0.4}N$ in lithium transition metal nitrides involve their layered structure and low oxidation state of the transition metal. In the meantime, more attention has been focused on understanding the electrochemical reactions of these transition metal compounds with Li. For example, Horn et al. investigated the lithium reaction mechanism of FeS_2 pyrite and found the formation of platelike Li_2S (plate thickness on the order of 20 nm) and Fe.[8] In general, the anions in transition metal compounds are believed to play an important role in the electrochemical reactions and provide the redox active centers on the anionic network, while the transition metal in these compounds is used to enhance surface electrochemical reactivity due to their nanoparticles less than 5 nanometers in the charging process.[3] It has been expected that the transition metal compounds can be used as anode materials to improve the performance of a lithium ion battery. However, the electrochemical reaction mechanism of transition metal compounds with lithium is still ambiguous. It is a challenge to synthesize novel negative electrode materials instead of the presently used carbonaceous negative electrodes.

Metal nitrides have excellent properties of high melting point and chemically inert behavior. It is advantageous for anode or cathodic materials to protect from moist or erosive environments. In fact, many original studies on the electrochemical reactions of metal nitrides with Li referred to Sn_3N_4 and Zn_3N_2.[9−11] Bates et al. have used them as anode materials for all solid-state thin film batteries.[10] Pereira et al. reported that the electrochemistry of Zn_3N_2 and its reaction mechanism with lithium was identified as a conversion reaction of Zn_3N_2 into LiZn alloy and a matrix of β-Li_3N. Interestingly, they also reported that a similar conversion reaction of Cu_3N with Li and Cu_3N electrodes exhibited good cycle life and excellent rate capabilities.[11] However, there is no available report on the electrochemical properties of metal nitrides of Co_3N and Fe_3N. Both nitrides of Co_3N and Fe_3N have a hexagonal structure, which is the same as that of α-Li_3N or β-Li_3N.

There have been several reports concerning preparation and microstructure of transition metal nitrides of Co_3N and Fe_3N in the past decades,[12−14] in which magnetron sputtering was used to deposit these thin films. Due to the inactivity of nitrogen gas, it is not easy to cause transition metal nitridation. In this paper, we report experimental results on the thin film fabrication of transition metal nitrides of Co_3N and Fe_3N deposited by using reactive pulsed laser ablation of a metallic target in a nitrogen ambient, and their electrochemical properties were first investigated. We also proposed a new electrochemical reaction mechanism of Li with transition metal nitrides.

Experimental Section

A new reactive film deposition system consisted of DC discharge and pulsed laser deposition. Thin films of transition metal nitrides were deposited by pulsed laser ablation of metallic targets combined with N_2 gas DC discharge at 100 mTorr. A 355 nm laser beam, provided by the third harmonic frequency of a Q-switched Nd:yttrium aluminum garnet (YAG) laser (Quantua Ray GCR-150), was used to irradiate the metallic cobalt or iron (99.99%) target with a fluence of 4 J/cm^2. The repetition rate and pulse width of the laser was 10 Hz and 6 ns,

* Corresponding author. E-mail: zhengwen@sh163.net.

10.1021/jp030530s CCC: $27.50
Published on Web 01/22/2004

respectively. The base pressure in the deposition chamber were 10^{-3} Pa. To produce reactively active nitrogen in the reaction chamber, a couple of copper discharge plates were installed between the target and substrate. DC bias can be applied to the copper plates to accelerate electrons in the ablation plume and activate nitrogen gas discharge. The activated nitrogen gas conditions provide the possibility of incorporating the reaction of nitrogen with these ablated transition metal species. The copper plate electrode was applied at about 650 V. The ambient N_2 gas pressure was kept at 30 Pa during the deposition. The used substrate was stainless steel sheet or coated indium−tin oxide (ITO) glass, and it was 25 mm away from the target. The substrate temperature was about 200 °C.

X-ray diffraction (XRD) patterns and the morphology of the thin film electrodes were recorded by a Rigata/max-C diffractometer with Cu Kα radiation and scanning electron microscopy (SEM) (Cambridge S-360), respectively. The film thickness was measured by a profilometer (Tencor Alpha-Step 200) and SEM. The weights of thin films were examined by electrobalance (BP 211D, Sartorius). X-ray photoelectron spectroscopy (XPS) measurements were performed on a Perkin Elmer PHI 6000C ECSA system with monochromatic Al Kα (1486.6 eV) irradiation. To correct possible charging of the films by X-ray irradiation, the binding energy was calibrated using the C1s (284.6 eV) spectrum of hydrocarbon that remained in the XPS analysis chamber as a contaminant. Since XPS is a surface-sensitive technique, care must be taken in the handling of the lithiated and delithiated samples. To avoid exposure to oxygen or water, the lithiated and delithiated films were rapidly transferred into the XPS chambers for the ex-situ XPS measurements. In addition, to check the surface cleanliness, the XPS spectra of sample surfaces before and after the bombardment by Ar ion for about 15 min were recorded. The lithiated or delithiated thin film electrodes were obtained by discharging to 0.01 V or charging to 3.5 V at a constant current of 5 μA/cm^2, and then were rinsed in anhydrous DMC to eliminate residual salts in an Ar-filled drybox.

For the electrochemical measurements, the cells were constructed by using the deposited thin films of metal nitrides as a working electrode and two lithium sheets as a counter electrode and a reference electrode, respectively. The electrolyte consisted of 1 M $LiPF_6$ in a nonaqueous solution of ethylene carbonate (EC) and dimethyl carbonate (DMC) with a volume ratio of 1:1 (Merck). The cells were assembled in an Ar-filled glovebox. Charge−discharge measurements were performed at room temperature with a Land BT 1-40 battery test system. The cells were cycled between 0.01 and 3.5 V vs Li/Li$^+$ at a current density of 7 μA/cm^2. For in-situ spectroelectrochemical measurements, thin films of metal nitrides deposited on the coated indium−tin oxide (ITO) glass were used as a working electrode. The electrochemical cell consisted of one pair of glass windows with an H form, in which the counter electrode and reference electrode were placed. A couple of quartz windows were sealed in another tube with the working electrode; the detected light beam with a diameter of about 4 mm can pass through the quartz window and be focused on thin films of metal nitrides. In-situ absorbance spectra of the electrochemical cell including quartz windows, electrolyte, and working electrode were measured by a BTC100E thermoelectric cooled linear charge-coupled device (CCD) spectrophotometer (B & W TEK INC.). Cyclic voltammogram measurements were performed with a CHI 660a electrochemical working station (CHI Instruments, TN).

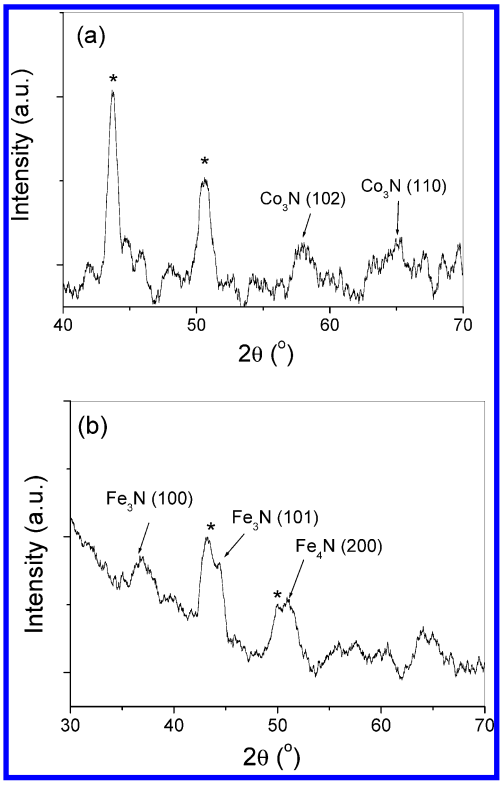

Figure 1. X-ray diffraction patterns of the as-deposited thin film of metal (a) Co and (b) Fe nitrides. The peaks marked with an asterisk correspond to stainless steel substrate.

Results and Discussion

Deposition and Characterization of Thin Films. The growth of transition metal nitride requires the presence of active nitrogen atoms or ions and high energetic metal flux. It is known that pulsed laser ablation with a metal target could generate an energetic metal flux above 100 eV.[15−16] The nitridation reaction of a transition metal can be considered to proceed according to the following steps:

$$N_2 + e \leftrightarrow 2N^* \quad (1)$$

$$N^* + x\mathrm{Fe} \rightarrow \mathrm{Fe}_x\mathrm{N} \quad (2)$$

$$N^* + x\mathrm{Co} \rightarrow \mathrm{Co}_x\mathrm{N} \quad (3)$$

Here, activated nitrogen atoms N* are produced by DC discharge in the laser plasma plume, and transition metal Fe and Co atoms are delivered by pulsed laser ablation of metal targets. Under our experimental conditions, the reactive deposition time was fixed to be about 2 h, and the thickness of as-deposited thin films was estimated to be about 300 ± 30 nm. The structure and composition analysis of the as-deposited thin films were characterized by XRD, XPS, and SEM measurements. Figure 1 depicted the X-ray diffraction patterns of the as-deposited films on the stainless steel substrate. Besides the diffraction peaks of $2\theta = 43.6°$ and 50.6° corresponding to the stainless steel substrate, two weak (102) and (110) diffraction peaks of the hexagonal γ-Co_3N[3] were observed in Figure 1a, indicating the presence of Co_3N. The main diffraction peaks in Figure 1b coincide with those from a hexagonal structure of Fe_3N[17] and a minor phase of Fe_4N.[18] The laser ablation fluence and nitrogen gas pressure should be responsible for the predominance of Co_3N and Fe_3N in pulsed laser reactive deposition.

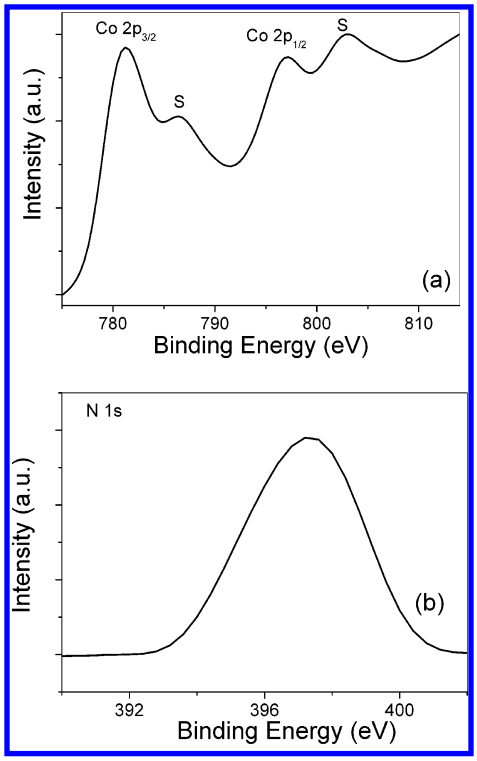

Figure 2. XPS spectra of the as-deposited thin film of cobalt nitride, (a) Co 2p and (b) N 1s.

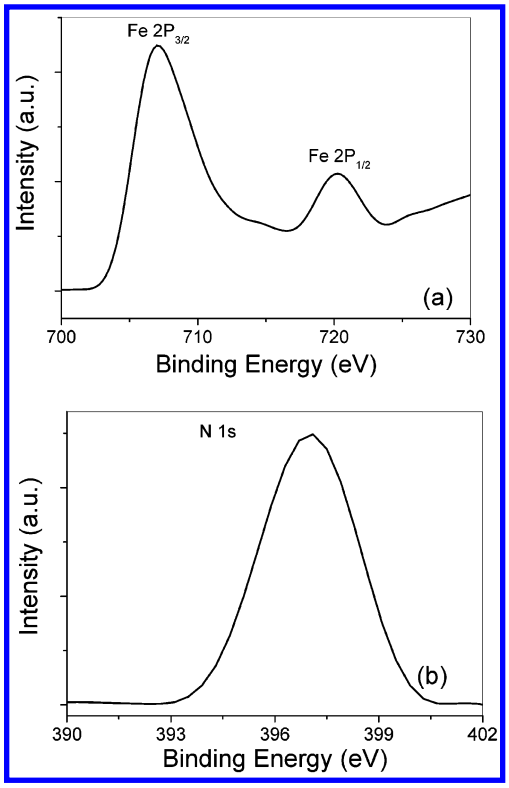

Figure 3. XPS spectra of the as-deposited thin film of iron nitride, (a) Fe 2p and (b) N 1s.

The formation of transition metal nitrides was further confirmed by XPS measurement. Figure 2 shows Co 2p and N 1s core level spectra of the as-deposited thin film. The electron binding energies peaked at 781.1 and 797.0 eV were assigned to be Co $2p_{3/2}$ and $2p_{1/2}$, respectively, in which two small satellites were also observed. The binding energies of the Co $2p_{3/2}$ electrons are found to be in the range from Co^0 (metal Co $2p_{3/2}$→ 778.2 eV) to Co^{2+}(781.8 eV).[19] A N 1s peak was observed at the binding energy of 397.2 eV, indicating cobalt nitride formed by nitridation of metal Co. The atomic concentration ratio of Co to N is estimated to be 3.0:1 by integrating the peaks area with their sensitivity factors (N: 0.38; Co: 4.5). This result indicates that the transition metal Co is reacted with N atom to form Co_3N, which is also supported by XRD data mentioned above.

Both Fe 2p and N 1s photoelectron core level spectra were shown in Figure 3. The binding energy peaked at 707.1 and 720.0 eV can be attributed to Fe $2p_{3/2}$ and Fe $2p_{1/2}$, respectively. The N 1s peak appears around 397.1 eV. According to the peaks area of Fe and N and their sensitivity factors (Fe: 3.8; N 0.38), the atomic concentration ratio of Fe to N is estimated to be 3.3:1. This is in agreement with the XRD data, in which the main composition of the as-deposited film should be Fe_3N with a minor Fe_4N.

Figure 4 shows the typical SEM images of the as-deposited Co_3N and Fe_3N films. These thin films exhibit a well-defined surface texture, and they are composed of very small crystalline grains uniformly distributed with an average size of 30−50 nm, indicating the nanostructure of the films. In addition, some particle agglomerates can be reviewed from SEM pictures. Similar images could be observed for other metal oxides deposited by the pulse laser ablation method,[20] and these pictures seem to be the feature of pulsed laser deposited thin film.

Electrochemical Reactions. Figure 5, parts a and b, show the charge and discharge curves for Li/as-deposited Co_3N and Li/Fe_3N thin film cells, respectively. Two cells were cycled

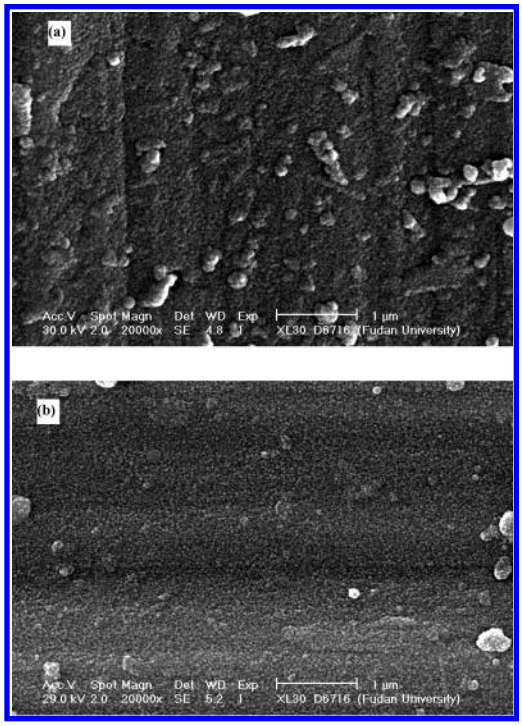

Figure 4. SEM images of the as-deposited thin film of metal (a) Co and (b) Fe nitrides.

between 0.01 and 3.5 V at a constant current density of 7 μA/cm^2. Weights of two as-deposited Co_xN and Fe_xN thin films were, respectively, estimated to be 0.25 ± 0.02 mg and 0.21 ± 0.02 mg on the substrates by using an electrobalance. These two cells have the same initial open-circuit voltage at 2.8 V, and the specific capacities of the first discharge were found to be above 400 mAh/g which should be equivalent to 3 Li per Co_3N or Fe_3N; their subsequent capacities fluctuate from 324

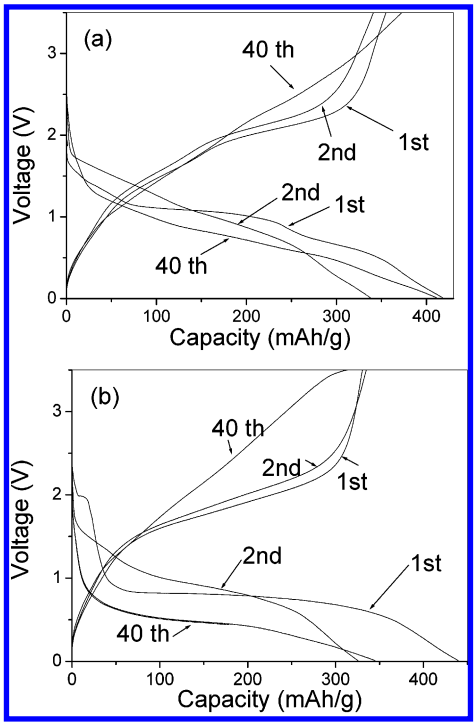

Figure 5. The discharge and charge curves of (a) Co_3N and (b) Fe_3N as anodes in lithium rechargeable batteries: Metal nitrides/ 1M LiPF6, EC-DEC (1:1)/Li.

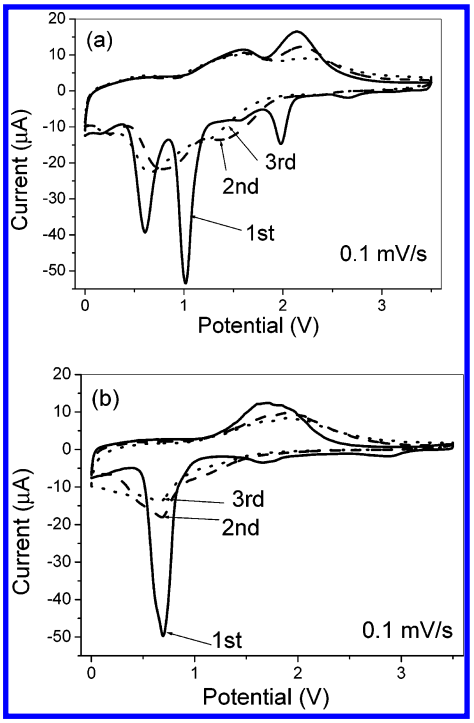

Figure 6. The first three cyclic voltammograms for the as-deposited film electrode of (a) Co_3N and (b) Fe_3N measured at a scan rate of 0.1 mV/s.

mAh/g to 420 mAh/g for the Co_3N thin film electrode, and from 323 mAh/g to 440 mAh/g for the Fe_3N thin film electrode, respectively. It is interesting to note that the discharge capacities after several cyclings are gradually close to the first discharge capacity during the first 40 cycles. The discharge capacity in the second discharge seems to exhibit a large difference from the first discharge, and there is apparent shape difference between the first discharge curve and the subsequent discharge curve for two cells. During the first discharge of a Co_3N thin film electrode, two different sloping voltages range from 1.07 to 0.97 V and from 0.75 to 0.55 V, but in the following discharge the sloping voltages occur in the ranges from 1.75 to 0.93 V and 0.92 to 0.69 V. The plateaus in the second and the subsequent discharge curves are similar, but different from the first one. These results imply that an irreversible process may occur in the first discharge.

Comparing with the first and second discharge curves of the Fe_3N thin film electrode, the sloping voltages from 2.12 to 0.97 V in the first discharge disappear in the second discharge, indicating that this is an irreversible process. Another sloping voltage occurs in the range from 0.83 to 0.75 V in the initial discharge; the subsequent discharge plateau at a voltage higher than the initial discharge can be due to the polarization.

Figure 6 shows the first three cyclic voltammograms for the as-deposited film electrode of Co_3N and Fe_3N between 0.01 and 3.5 V measured at a scan rate of 0.1 mV/s, respectively. For the Co_3N thin film electrode, three cathodic current peaks at 1.97 V, 1.02 V, and 0.60 V are observed in the first cycle. But in the second cycle, two peaks appear at 1.40 V and 0.67 V. The anodic peaks located at 1.8 V and 2.1 V remain unchanged. These results imply that the electrochemical process taking place in the first discharge is different from the subsequent processes. However, two small cathodic peaks at 2.87 V and 1.70 V in the first cycle of the Fe_3N thin film electrode disappear in the subsequent cycles and these peaks could be attributed to an irreversible process. Another cathodic peak at around 0.70 V in the first cycle and this peak remain unchanged after subsequent cycles. In all charging processes, there is an anodic peak at 1.70 V to be observed. The discharge/charge and cyclic voltammogram measurements for the two cells are in good agreement and indicate that the electrochemical processes in the second and subsequent cycles are different from the process in the first one.

In-Situ Spectroelectrochemical Characterization. The color of the thin film is one of its physical features and is related to the structure and composition of thin film material. Co_3N thin film deposited onto ITO glass is colorless and transparent over the visible region. However, the as-deposited Fe_3N thin film on ITO glass seems to have a weak yellow color. Since the structure changes and new products occur in the electrochemical reaction of transition metal nitride films with lithium, this will result in different optical absorption characteristics.

Figure 7, parts a and b, show the three-dimensional planform of in-situ absorbance spectra collected at various x values in Li_xCo_3N and x values as a function of potential in the initial discharge, and charge processes are shown in the right figures, respectively. For the initial discharge and charge processes, a progressive increase and decrease of the in-situ absorbance are observed when the Li ions are reduced down to 0.01 V and further oxidized up to 3.5 V, respectively. The shapes of absorbance spectra are dependent on the x values, and there seem to be two absorption bands at 750 nm and around 600 nm—the absorption band around 600 nm shows a red-shift with increasing x. When the absorbance values at 600 nm are more than 0.5, the color of the lithiated thin film electrode could be viewed by the naked eye and becomes apparently black. During the charging process, the thin film electrode still remains black, while there is a little change in the absorbance spectra as shown in Figure 7b. The color change and absorbance spectra of the as-deposited thin film electrode strongly verify the lithiation or delithiation reaction processes.

To further examine the relation between the absorbance and x values in the initial discharge and charge processes, the absorbance at 600 nm as a function of the x values are presented

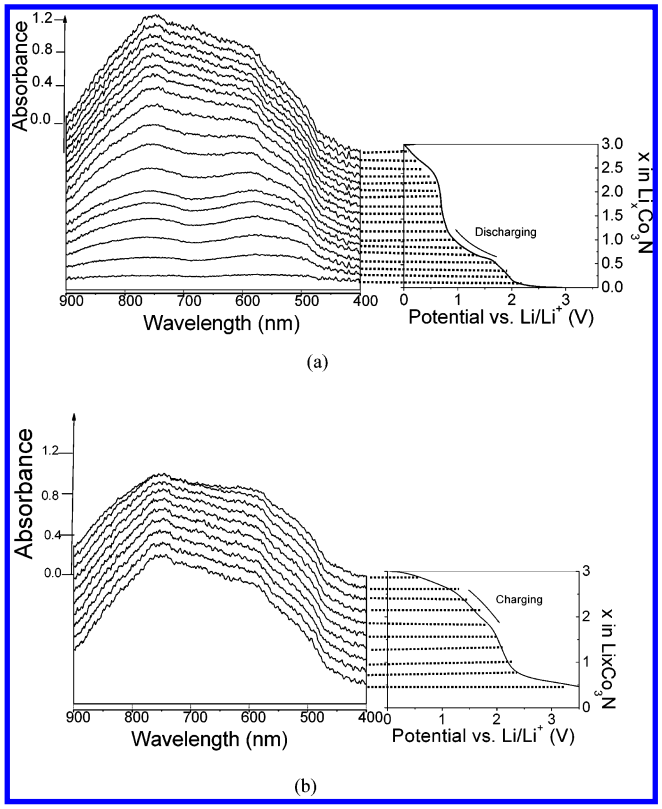

Figure 7. The three-dimension planform of selected in-situ absorbance spectra (left figure) obtained (a) during first discharging of Co_3N to 0.01 V and (b) during charging of Co_3N to 3.5 V under a constant current 7 $\mu A/cm^2$. Every state in the initial discharge or charge cycle to record these spectra was shown in the right figures. The *x* values correspond to the number of Li reaction per Co_3N.

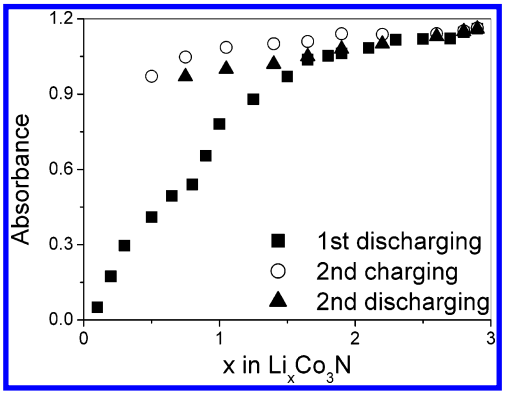

Figure 8. Absorbance at 600 nm vs the *x* values of Li reacted number per Co_3N.

in Figure 8. It can be seen that the absorbance values change from 0 to 1.16, corresponding to *x* values from 0 to 3 in the first discharging process. During the charging process, the absorbance values are in the range from 0.97 to 1.16, corresponding to *x* values from 0.5 to 3.0. The absorbance values are more than 0.97, and the color of the thin film electrode remains black in the second discharging process. The absorbance changes in discharge and charge processes exhibit an irreversible feature similar to their electrochemical reaction behavior.

A similar spectroelectrochemical behavior was also found for the Fe_3N thin film electrode. Figure 9 shows the absorbance at 600 nm as a function of the *x* value in Li_xFe_3N. It can be seen that the absorbance values remain around 1.6 when the *x* Li values change from 0.7 to 3.0 during the charging and the second discharging processes. These results provide evidence that the

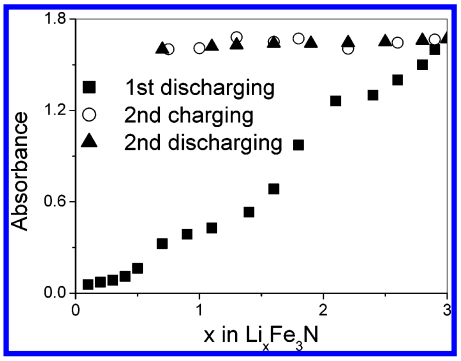

Figure 9. Absorbance at 600 nm vs the *x* value of Li reacted number per Fe_3N.

lithiation reaction occurs in the discharge process, while a subsequent delithiation reaction is irreversible with regard to the first lithiation and the relithiation reaction is strongly different from the first lithiation.

Characterization of Lithiated and Delithiated Thin Film Electrodes. The ex-situ XRD, XPS, and SEM measurements of lithiated and delithiated thin film electrodes were performed in order to get insight into the reaction mechanism of transition metal nitrides with lithium. Figure 10, parts a and b, show X-ray diffraction patterns of Co_3N and Fe_3N thin film electrodes obtained at lithiated and delithiated states, respectively. When discharging to 0.01 V, metal Co(111) peaked at 44.3° and metal Fe(110) peaked at 44.6° emerge in the XRD patterns. More interesting, if charging to 3.5 V, small XRD peaks from metal Co(111) and Fe(110) are still observed. Apparently, the lithiation products of metal Co and Fe are formed during the discharging process, but they were not entirely nitrided during the charging process. In other words, delithiated products are not converted into the original composition of Co_3N and Fe_3N in the subsequent cycling.

A further confirmation was performed by the ex-situ XPS measurements. Figure 11, parts a and b, presents Co 2p spectra of lithiated and delithiated Co_3N thin films before and after the bombardment, respectively. It can be seen that XPS spectra before and after the bombardment by Ar ions are different, indicating the surface contamination due to the exposure to oxygen or water. Thus, XPS data will be mainly analyzed for those after the bombardment by Ar ions. As shown in Figure 11a, Co 2p peaks at 777.8 and 792.5 eV with two small satellite peaks could be assigned to the Co 2p spectrum from metal Co,[21−22] which is distinctly different from the XPS spectrum of the as-deposited film. The electron binding energy of Co $2p_{3/2}$ shifting toward a low energy of 2.3 eV implies the formation of metallic cobalt during electrochemical reaction of Co_3N with Li. The $2p_{3/2}$ and $2p_{1/2}$ XPS spectra of the delithiated Co_3N thin film shown in Figure 11b peak at 781.9 and 795.3 eV. Definite assignment to the delithiated products is uncertain as a result of the complexity of the 2p XPS spectrum feature,[22−26] but the 2p spectrum of the delithiated thin film is apparently different from that of the lithiated and the as-deposited Co_3N thin film. This result suggests that the metallic Co converts into other cobalt nitrides such as CoN or Co_2N instead of Co_3N during charging of the Co_3N /Li cell. These results are consistent with XRD data of lithiated and delithiated products.

Figure 12, parts a and b, present Fe 2p spectra of the lithiated and delithiated Fe_3N thin films before and after the bombardment, respectively. The large difference of the Fe 2p spectrum between pre- and post-bombardment of the lithiated Fe_3N thin film indicated the surface of lithiated products is easily

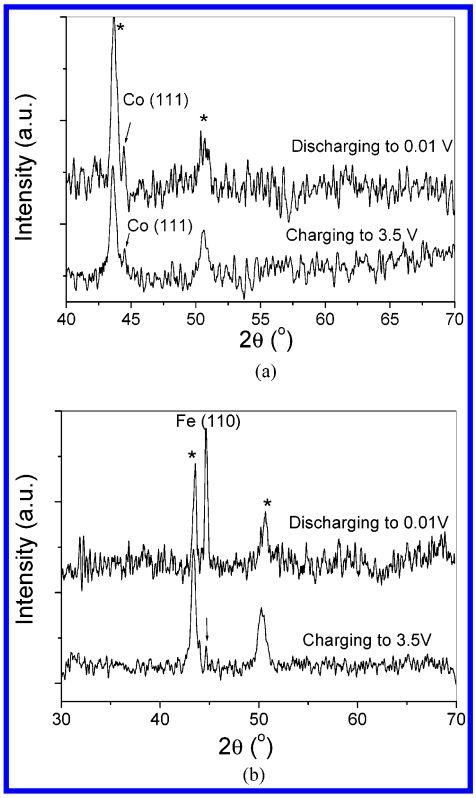

Figure 10. The ex-situ XRD patterns of the lithiated and delithiated thin film of (a) Co_3N and (b) Fe_3N.

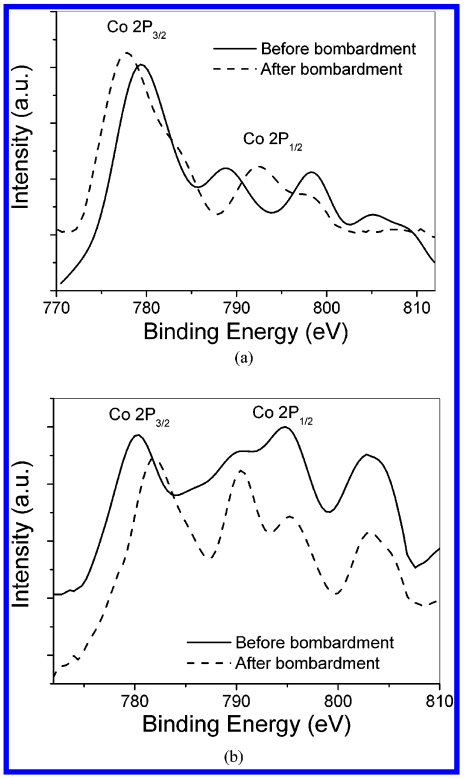

Figure 11. Both Co 2p XPS spectra of (a) the lithiated and (b) delithiated thin films of Co_3N before and after bombardments by Ar ions about 15 min.

contaminated or oxidized. For the film sample after the bombardment by Ar ion, the Fe 2p spectra of the lithiated thin film electrode consist of single peak Fe $2p_{3/2}$ and Fe $2p_{1/2}$ appearing at 707.1 and 720.5 eV, respectively, which seem nearly the same as that of the as-deposited thin film. In addition,

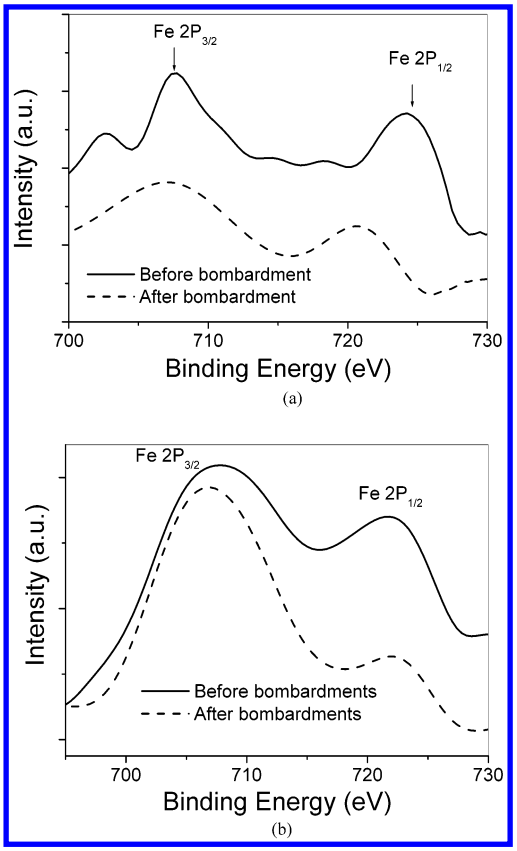

Figure 12. Both Fe 2p XPS spectra of (a) the lithiated and (b) delithiated thin films of Fe_3N before and after bombardments by Ar ions about 15 min.

the Fe 2p XPS spectrum of the delithiated thin film shows a similar feature, but the lithiated thin film has larger full width at half-maximum (fwhm) than the delithiated thin film. Previous studies[26,27] on the XPS of Fe and Fe_3N showed that there is not a measurable chemical shift for the binding energy Fe $2p_{3/2}$ and $2p_{1/2}$ of Fe and Fe_3N; the Fe $2p_{3/2}$ signal has been in the range 706.5−707.1 eV for metallic Fe, 709.5−710.3 eV for Fe(II), and 710.6−711.4 eV for Fe(III). So we could reasonably assume that the Fe 2p XPS spectrum of the lithiated thin film should be assigned to Fe. The as-deposited and delithiated thin films show different shapes of the Fe 2p XPS spectrum and both spectra should be attributed to different Fe chemical states less than Fe(II).

As shown in Figures 13 and 14, both Li 1s and N 1s XPS spectra of the lithiated Co_3N and Fe_3N thin film electrodes before and after the bombardment are nearly the same. These results indicated that the effect of an Ar bombardment on the chemistry of lithiated samples is less. The same Li 1s and N 1s XPS values for the lithiated Co_3N and Fe_3N thin film electrodes indicated the existence of Li_3N in two lithiated products.

SEM studies of lithiated Co_3N and Fe_3N thin films after the second discharging are presented in Figure 15, parts a and b. Compared with the morphology of the as-deposited thin films, the sizes of the grains after lithiating become larger. Their mean sizes on the surface of the lithiated film are estimated to be in the range of 80−110 nm, which is most likely due to the agglomeration of nanosized particles and the electrolyte interface surrounding the agglomerates. The changes of the morphology and sizes of surface particles suggest that the as-deposited nanosized particles take part in the electrochemical reaction with Li.

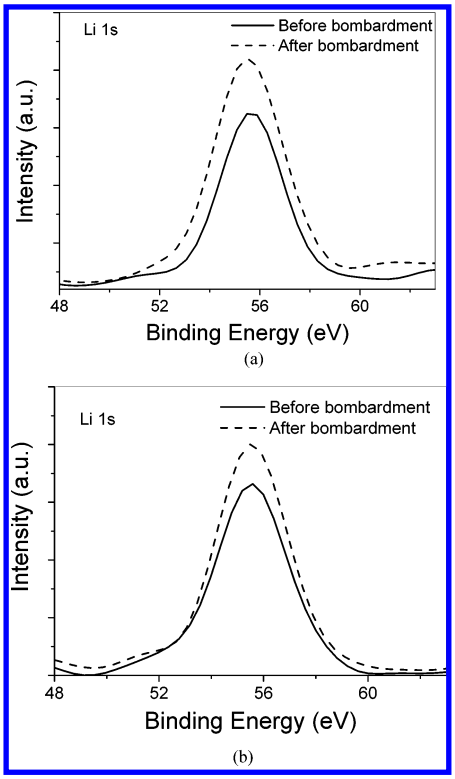

Figure 13. Both Li 1s XPS spectra of the lithiated thin films of (a) Co_3N and (b) Fe_3N before and after bombardments by Ar ions about 15 min.

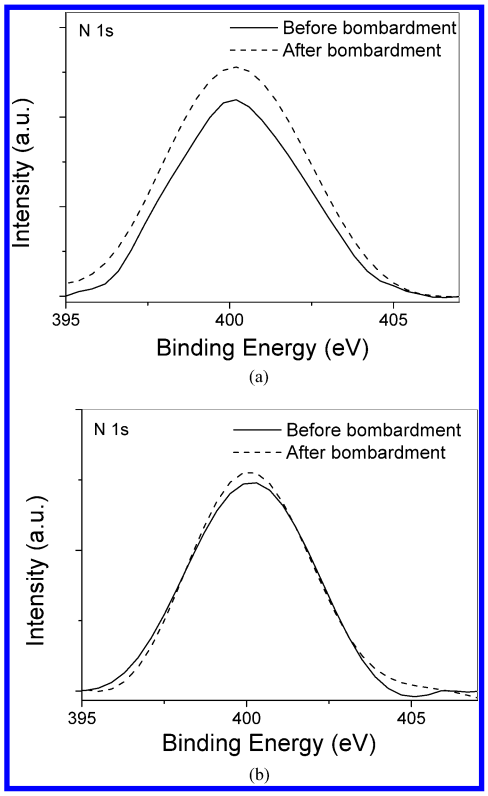

Figure 14. Both N 1s XPS spectra of the lithiated thin films of (a) Co_3N and (b) Fe_3N before and after bombardments by Ar ions about 15 min.

Discussion. Table 1 summarizes the experimental XPS data for the as-deposited, lithiated, and delithiated thin films, and compares these data with the data for transition metal oxides. It can be seen that the XPS data of Co, Fe, and N change after lithiation and delithiation. These changes strongly support the

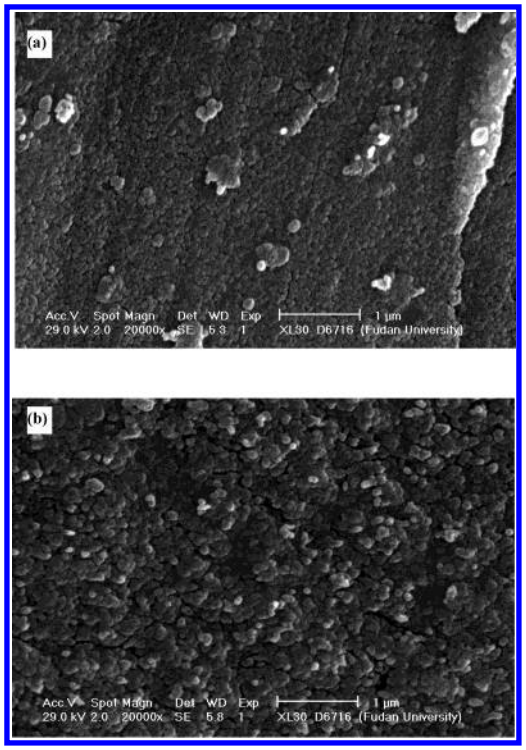

Figure 15. SEM images of the lithiated thin film of (a) Co_3N and (b) Fe_3N.

electrochemical process occurring. After lithiation, metallic Co and Fe were found in the lithiated thin film electrode of Co_3N and Fe_3N from the XPS and XRD data. In addition, the Li 1s XPS spectrum of the lithiated electrode also indicates the formation of Li_3N. It is obvious that metallic Co and Fe and Li_3N are produced from the electrochemical reactions of nanocrystalline Co_3N and Fe_3N with Li, and those reactions during the first discharging process might be expressed as follows:

$$M_3N + 3Li^+ + 3e^- \rightarrow Li_3N + 3M \qquad (4)$$

Here, M is metallic Co and Fe. From reaction 4, the theoretical capacities for Co_3N and Fe_3N could be estimated to be 421 mAh/g and 443 mAh/g, respectively. These values are close to the reversible capacity of around 400 mAh/g in our discharge and charge data. It should be unambiguous to understand a Li-driven decomposition of metal composites into the metallic M particles dispersed into the Li_3N matrix. In general, the metallic M particles must be of nanosized dimension and they are well below the limit of detection in XRD measurement. For example, Poizot et al. reported the lithium reactions of transition metal oxides. No diffraction peaks from metallic Co in the XRD pattern were observed. They assumed that in-situ formation of metal nanoparticles during the first discharge smaller than the X-ray coherence length (in the range 1−5 nanometer) enables the formation and decomposition of Li_2O upon subsequent cycling.[3] Pralong et al. reported the XRD pattern of the products after the first discharge of the lithium reaction of CoP_3, and there are no diffraction peaks observed from those of metallic cobalt.[4] Recently, we could also not observe the diffraction peaks of metallic Zn and Li_2O at the lithiation process of Li reacted with ZnO corresponding to 2 Li per Zn atom by the ex-situ XRD measurements.[19] However, our present results provide a special case, and there are clear diffraction peaks from metal Co(111) and Fe(110) in the lithiated thin films. Obrovac and Dahn et al. collected XRD data of the lithiated $LiFeO_2$ and CoO for 12 h, broad peaks of Fe(110) and Co(111) were observed;[28]

TABLE 1: A Comparison between the XPS Values for Transition Metal Oxides and the As-Deposited, Lithiated, and Delithiated Nitrides[a]

		as-deposited	lithiated	delithiated	M	MO	M_2O_3
Co_3N	Co $2P_{3/2}$	781.1 eV	777.8 eV	781.9 eV	778.2 eV[b]	781.8 eV[b]	779.6 eV[b]
	N 1s	397.2 eV	400.1 eV	397.3 eV			
	Li 1s		55.6 eV	55.3 eV			
Fe_3N	Fe $2P_{3/2}$	707.1 eV	707.1 eV	707.1 eV	706.7−707.1 eV[c]	709.5−710.3 eV[c]	710.6−711.4 eV[c]
	N 1s	397.1 eV	400.1 eV	397.2 eV			
	Li 1s		55.6 eV	55.3 eV			
	TW	TW	TW	TW	ref.	ref.	ref.

[a] M is Co or Fe; TW is this work. [b] Ref 19. [c] Ref 26−27.

these reports about diffraction peak positions are the same as observed Co(111) and Fe(110) in our XRD pattern. But the crystalline sizes of metallic Co and Fe in the lithiated Co_3N and Fe_3N thin films calculated by Scherrer's formula[29] are found to be 25 nm from their widths of XRD peaks in Figure 10. It is interesting to note that the lithiation reaction of Co_3N and Fe_3N produce a good crystallinity of metallic Co and Fe (at least with respect to X-rays).

The XRD patterns of delithiated Co_3N and Fe_3N thin films show that part of the metallic Co and Fe remains in the delithiated products, and there are not any other diffraction peaks except from the substrate. It means that the delithiated thin films could not resume their original structures of the as-deposited thin films. The in-situ spectroelectrochemical data showed that the changes of the color and absorbance spectra are irreversible for the discharging and charging processes. The Co 2p and Fe 2p XPS spectra of the delithiated thin films are also different from those of the as-deposited thin films. Thus the charging process is an irreversible process with regard to the first discharging process. The possible electrochemical reaction during the subsequent process is proposed as follows:

$$3M + Li_3N \leftrightarrow (3 - y)M + M_yN + 3Li \qquad (5)$$

Here M is transition metallic Co and Fe, and y is less than 3. This reaction can explain the CV data and the in-situ spectroelectrochemical measurements, in which the electrochemical processes in the second and subsequent cycles are different from the first one. Recently, Prosini et al. studied the electrochemical characterization of mixtures of ball-milled lithium nitride and iron metal with the Li_3N/Fe ratio from 2 to 8; their results showed that iron is not directly involved in the electrochemical reaction and the electrochemical performance of the composite electrode can be totally ascribed to Li_3N.[30] The discharge curves of Co_3N and Fe_3N thin films are different from their data. Thus, their results are strongly different from our case. There is clearly change between the diffraction intensities from the metal Co-(111) and Fe(110) XRD patterns of the lithiated and delithiated Co_3N and Fe_3N thin films in our case, indicating that part of the metallic Co and Fe in the lithiated products takes part in the electrochemical reaction in the discharging process.

The lithium reactive mechanism in the transition metal oxides has been proposed by Tarascon et al. In-situ formation of metal nanoparticles less than 6 nm during the first discharge led to the conclusion that the reversible formation and decomposition of Li_2O could be driven by nanosized transition metals. However, the nanosizes of transition metallic Co and Fe in the lithiated products of Co_3N and Fe_3N are more than 6 nm in our case. Thus, the reversible formation and decomposition of Li_3N could be driven by metal nickel particles more than 5 nm in our case. It provides a new reaction mechanism, which may be related to the rich transition metal in Co_3N and Fe_3N with low metal oxidation states. After lithiating, these reduced rich metals form a good crystallinity, and they are easily detected by XRD measurement. The rich transition metals dispersed into the containing lithium matrix (Li_3N) may be helpful in driving the decomposition of Li_3N.

Since it is difficult to detect Li_3N due to its small particle size and the atomic scattering factors of Li and N lower than that of transition metal, the lithium nitrides of α-Li_3N or β-Li_3N were not observed in the ex-situ XRD patterns. However, they could be confirmed by the ex-situ XPS measurements. The as-deposited Co_3N and Fe_3N thin films have the same hexagonal structure as α-Li_3N or β-Li_3N. When the Li ions are driven into transition metal nitrides during the discharging process, and close to N and will react with the N atoms in the framework of the Co_3N and Fe_3N structure. The Li−N bonds are gradually formed instead of Co−N or Fe−N bonds to form Li_3N. In the meantime, the Li can occupy the position of Co or Fe in metal nitrides; the metallic Co or Fe may be pushed out by the Li displacive reaction. A similar displacive mechanism to account for the electrochemical reaction of lithium with CoO was suggested by Obrovac and Dahn et al.; they considered that the original lithium oxide oxygen lattice is preserved and the reaction resembles an ion exchange process.

According to the data from Table 1, N 1s binding energies peaked at 397.2 eV for the Co_3N and Fe_3N shift toward the high-energy position at 400.1 eV after the lithiation process, indicating that N takes part in an electrochemical reaction. From eq 4, during the first discharging process, the anion N in the transition metal nitrides as a reactive center may determine the discharge capacity. However, the transition metallic Co and Fe should play an important role in the subsequent lithiation reaction. One part of metallic Co and Fe is nitrided to form nitrides such as M_2N or MN, different from Co_3N and Fe_3N, and Li is released. Another part of metal Co and Fe in the lithiated and delithiated products seems to act as an active spectator upon reformation of Li_3N from eq 5; a similar role of transition metal as an active spectator has been noted by Pralong and Tarascon et al.,[4,31] and the role in the redox process is still unclear at the present time. It is expected that the existence of metallic Co and Fe as an active spectator in the lithiated and delithiated products can provide good electronic conductivity to improve the lithium electrochemical reaction rate. On the other hand, it may be advantageous for the transition metal dispersed into the containing lithium matrix (Li_3N) to drive the decomposition of Li_3N. Thus, two kinds of roles of metallic Co and Fe in the reversible lithium electrochemical reaction are revealed and should be responsible for their characteristics of electrochemical behavior. The origin of the reversible capacity fluctuation with cycle number for Li/the as-deposited Co_3N and Fe_3N thin film cells should be rather complicated, but the reaction between the surface of transition metal particles and electrolyte may be involved. It needs more powerful experimental techniques for clarification in future work.

Conclusions

In this paper, thin films of transition metal nitrides have been successfully prepared by a reactive pulsed laser deposition method with DC discharge in nitrogen ambient. The lithium electrochemical reactions of Co_3N and Fe_3N thin films have the same feature, and these thin film electrodes exhibit the reversible discharge capacity in the range from 324 mAh/g to 420 mAh/g. The in-situ spectroelectrochemical data also showed the lithiation reaction of Co_3N and Fe_3N thin films. The diffraction peaks from metal Co(111) and Fe(110) in the lithiated thin film were observed by the ex-situ XRD measurement, and this evidence demonstrates the existence of metallic Co and Fe, which was further confirmed by the ex-situ XPS measurement. Their electrochemical reaction with Li could not be explained by the oxidation/reduction of nanosized metal due to the nanosize of well crystallized transition metallic Co and Fe more than 5 nm. The low transition metal oxidation states in the Co_3N and Fe_3N cause the transition metallic particles to disperse into the containing lithium matrix (Li_3N) after lithiating. One part of metallic Co and Fe is nitrided and reduced in the lithium electrochemical reaction; another part of Co and Fe seems to act as an active spectator to help drive the formation and decomposition of Li_3N. So this phenomenon may become a useful method for guiding the design and fabrication of novel materials.

Acknowledgment. The authors thank Professor Qi-ke Zheng for her discussion. This work was supported by the National Nature Science Foundation of China (Projects No. 20083001 and 20203006).

References and Notes

(1) Leroux, F.; Ouvrard, G. R.; Power, W. P.; Nazar, L. F. *Electrochem. Solid State Lett.* **1998**, *1*, 523.

(2) Denis, S.; Baudrin, E.; Orsini, F.; Ouvrard, G.; Touboul, M.; Tarascon, J. M. *J. Power Sources* **1999**, *81*, 79.

(3) Poizot, P.; Laruelle, S.; Grugeon, S.; Dupont, L.; Tarascon, J. M. *Nature* **2000**, *407*, 496.

(4) Pralong, V.; Souza, D. C. S.; Leung, K. T.; Nazar, L. F. *Electrochem. Commun.* **2002**, *4*, 516.

(5) Elder, S. H.; Doerrer, L. H.; Disalvo, F. J.; Parise, J. B.; Guyomard, D.; Tarascon, J. M. *Chem. Mater.* **1992**, *4*, 928.

(6) Rowsell, J. L. C.; Pralong, V.; Nazar, L. F. *J. Am. Chem. Soc.* **2001**, *123*, 8598.

(7) Takeda, Y.; Nishijima, M.; Yamahata, M.; Takeda, K.; Imanishi, N.; Yamamoto, O. *Solid State Ionics* **2000**, *130*, 61.

(8) Horn, Y. S.; Osmialowski, S.; Horn, Q. C. *J. Electrochem. Soc.* **2002**, *149*, A1547.

(9) Neudecker, B. J.; Zuhr, R. A.; Bates, J. B. *J. Power Sources* **1999**, *81*−*82*, 27.

(10) Bates, J. B.; Dudney, N. J.; Neudecker, B.; Ueda, A.; Evans, C. D. *Solid State Ionics* **2000**, *135*, 33.

(11) Pereira, N.; Klein, L. C.; Amatucci, G. G. *J. Electrochem. Soc.* **2002**, *149*, A262.

(12) Oda, K.; Yoshio, T. *J. Mater. Sci.* **1987**, *22*, 2729.

(13) Shih, K. K.; Karasinski, J. *J. Appl. Phys.* **1993**, *73*, 8377.

(14) Asahara, H.; Migita, T.; Tanaka, T.; Kawabata, K. *Vacuum* **2001**, *62*, 293.

(15) Hubler, G. K. In *Pulsed Laser Deposition of Thin Films*; Chrisey, D. B., Hubler, G. K., Eds.; Wiley: New York, 1992; pp 327−355.

(16) Qin, Q. Z.; Fu, Z. W. *Adv. Mater.* **1999**, *11* (13), 1119.

(17) *Z. Anorg. Chem.* **1945**, *253*, 95.

(18) Danke, M. F.; Worzala, F. J. *J. Sci. Forum* **1992**, *102*−*104*, 259.

(19) Mekki, A.; Holland, D. J.; Ziq, Kh.; Conville, Mc. C. F. *J. Non-Cryst. Solids* **1997**, *220*, 267.

(20) Fu, Z. W.; Huang, F.; Zhang, Y.; Qin, Q. Z. *J. Electrochem. Soc.* **2003**, *150*, A714.

(21) Mclntyre, N. S.; Cook, M. G. *Anal. Chem.* **1975,** *47*, 2208.

(22) Barr, T. L. *J. Phys. Chem.* **1978**, *82*, 1801.

(23) Hanawalt, *Anal. Chem.* **1938**, *10*, 475.

(24) Casella, I. G.; Guascito, M. R. *J. Electroanal. Chem.* **1999**, *746*, 54.

(25) Raquet, B.; Mamy, R.; Ousset, J. C.; Negre, N.; Goiran, M.; Piecourt, C. G. *J. Magn. Magn. Mater.* **1998**, *184*, 41.

(26) Alphonsa, I.; Chainani, A.; Raole, P. M.; Gangli, B.; John, P. I. *Surf. Coatings Technol.* **2002**, *150*, 263.

(27) Castro, V. D.; Ciampi, S. *Surf. Sci.* **1995**, *331*−*333*, 294.

(28) Obrovac, M. N.; Dunlap, R. A.; Sanderson, R. J.; Dahn, J. R. *J. Electrochem. Soc.* **2001**, *148*, A576.

(29) Cullity, B. D. *Elements of X-ray Diffraction*, 2nd ed.; Addison-Wesley: Reading, MA, 1978.

(30) Prosini, P. P.; Cardellini, F. *Electrochem. Commun.* **2002**, *4*, 853.

(31) Tarascon, J. M.; Morcrette, M.; Dupont, L.; Chabre, Y.; Payen, C.; Larcger, D.; Pralong, V. *J. Electrochem. Soc.* **2003**, *150*, A732.